EDGEWOOD
CHEMICAL BIOLOGICAL CENTER
U.S. ARMY SOLDIER AND BIOLOGICAL CHEMICAL COMMAND

ECBC-TR-209

ETHANOL DETECTION STRATEGY WITH MULTIPLE DIGITAL FILTERING OF PASSIVE FT-IR INTERFEROGRAMS

Patrick O. Idwasi
Gary W. Small

OHIO UNIVERSITY
Athens, OH 45701-2979

Roger J. Combs
Robert B. Knapp
Robert T. Kroutil

RESEARCH AND TECHNOLOGY DIRECTORATE

September 2001

Aberdeen Proving Ground, MD 21010-5424

Disclaimer

The findings in this report are not to be construed as an official Department of the Army position unless so designated by other authorizing documents.

REPORT DOCUMENTATION PAGE

Form Approved
OMB No. 0704-0188

1. AGENCY USE ONLY *(Leave Blank)*	2. REPORT DATE	3. REPORT TYPE AND DATES COVERED
	September 2001	**Final; 99 Oct - 00 Dec**

4. TITLE AND SUBTITLE
Ethanol Detection Strategy with Multiple Digital Filtering of Passive FT-IR Interferograms

5. FUNDING NUMBERS
PR-20150/CB2

6. AUTHOR(S)
Idwasi, Patrick O.; Small, Gary W. (Ohio University); Combs, Roger J.; Knapp, Robert B.; and Kroutil, Robert T. (ECBC)

7. PERFORMING ORGANIZATION NAME(S) AND ADDRESS(ES)
Chemistry and Biochemistry Department, Ohio University, Athens, OH 45701-2979

DIR, ECBC, ATTN: AMSSB-RRT-DI, APG, MD 21010-5424

8. PERFORMING ORGANIZATION REPORT NUMBER
ECBC-TR-209

9. SPONSORING/MONITORING AGENCY NAME(S) AND ADDRESS(ES)

10. SPONSORING/MONITORING AGENCY REPORT NUMBER

11. SUPPLEMENTARY NOTES

12a. DISTRIBUTION/AVAILABILITY STATEMENT
Approved for public release; distribution is unlimited.

12b. DISTRIBUTION CODE

13. ABSTRACT *(Maximum 200 words)*

Digital filtering methods are evaluated for automated detection of ethanol using passive Fourier transform infrared (FT-IR) data collected during laboratory and open-air experiments. In applications where ethanol signals are overlapped by spectral interference signals (e.g., ammonia and acetone), the use of multiple digital filters is found to improve the sensitivity of the vapor analyte detection. The detection strategy applies bandpass digital filters to short interferogram segments that are acquired from the passive FT-IR spectrometer configuration. To implement the automated detection of the ethanol target analyte, the filtered interferogram segments are input into a piecewise linear discriminant analysis. Through the use of a set of training data, discriminants are computed that are subsequently used for automated detection of ethanol vapor. A two-filter strategy with separate ethanol and ammonia filters is compared to a single ethanol filter approach. Bandpass parameters of the digital filters and the interferogram segment location are optimized with laboratory data. The laboratory data are generated for ethanol, ammonia, and acetone vapor mixtures in a gas cell, whose contents are viewed against various infrared background radiances. The optimized parameters, from the laboratory data, are subsequently tested with open-air remote sensing data. The open-air data consists of elevated temperature ethanol and ammonia plumes generated from a portable emission stack. The two-filter strategy outperforms the single-filter approach in laboratory and open-air scenarios, where the ammonia spectral interference dominates the ethanol spectral signature.

14. SUBJECT TERMS
FT-IR spectrometry **Pattern recognition** **Spectral interference**
Multiple digital filtering **Ethanol vapor detection**

15. NUMBER OF PAGES
35

16. PRICE CODE

17. SECURITY CLASSIFICATION OF REPORT	18. SECURITY CLASSIFICATION OF THIS PAGE	19. SECURITY CLASSIFICATION OF ABSTRACT	20. LIMITATION OF ABSTRACT
UNCLASSIFIED	**UNCLASSIFIED**	**UNCLASSIFIED**	**UL**

Blank

PREFACE

The work described in this report was authorized under Project No. 20150/CB2, Exploratory Development. The work was started in October 1999 and completed in December 2000.

The use of either trade or manufacturers' names in this report does not constitute an official endorsement of any commercial products. This report may not be cited for purposes of advertisement.

This report has been approved for public release. Registered users should request additional copies from the Defense Technical Information Center; unregistered users should direct such requests to the National Technical Information Center.

Acknowledgments

The authors would like to thank Charles T. Chaffin, Jr., and Timothy L. Marshall (Aerosurvey, Incorporated, Manhattan, KS) for their work in calibrating and operating the plume generator used in the two open-air experiments.

Blank

CONTENTS

FIGURES

TABLES

ETHANOL DETECTION STRATEGY WITH MULTIPLE DIGITAL FILTERING OF PASSIVE FT-IR INTERFEROGRAMS

1. INTRODUCTION

The monitoring of industrial stack effluents is important in the areas of implementing environmental regulations, detecting hazardous chemical releases, and maintaining quality control of industrial processes. Remote monitoring techniques apply to these areas because of the ability to monitor various scenes with a single sensor and the advantage of not needing to place the sensor in a harsh or hazardous environment. Desirable characteristics for a remote monitor include portability, ruggedness, fast data acquisition, automated operation, and the availability of real-time monitoring results.

Open-air Fourier transform infrared (FT-IR) spectrometry is being investigated as a potential analytical solution in the remote monitoring scenarios described above because it exhibits many of the properties of an ideal remote sensing technique.[1-5] Significant effort has been devoted to decreasing the size and weight of FT-IR instrumentation, as well as increasing its ruggedness, through improvements in sensor design. Corresponding improvements in computer and detector technology have increased the analytical sensor performance and have made automated real-time detection feasible.

The FT-IR remote sensing measurements have been implemented in either an active or passive mode. In the active mode, a controlled, high temperature infrared (IR) source is used to probe the atmosphere between either the source and spectrometer or between an external retroreflector and the source/spectrometer package. The passive experiment relies on an IR radiance differential between background and target vapor. The IR emission arises for elevated temperature gases relative to a colder background scene (i.e., source) radiances. On the other hand, IR absorption occurs for an atmospheric species relative to an elevated temperature background scene. The passive mode has the advantage of greater simplicity and flexibility in utility, but it often suffers the disadvantage of increased variability in the acquired data due to the dependence upon the uncontrolled background scene radiances.

Work in our laboratories has focused on demonstrating the viability of passive FT-IR remote sensing measurements through the development of data analysis algorithms. These algorithms allow compensation for the data variance associated with radical changes in the background radiance.[6-9] The strategy of the algorithms is applying digital filter techniques to specific segments of the raw interferogram data collected by the passive FT-IR spectrometer. This analysis approach takes advantage of the fact that the background radiance is primarily represented as a broad spectral feature. This broad background spectral feature is constrained to the region around the interferogram centerburst and near the point of zero path difference (ZPD). Spectral bands of target species such as volatile organic compounds are much narrower. These narrower spectral features correspond to a representation that is spread over a much large optical retardation in the interferogram. This distribution of the narrow spectral features has been demonstrated by passive remote detection of target compounds with short interferogram

segments of 120 points or less that are adequately displaced from the interfergram ZPD.[10] Restriction of the data acquisition to a short interferogram segment decreases data acquisition time and points to potentially more rugged interferometer designs.[11] A fast data acquisition time for a remote sensor permits a snapshot of the vapor analyte that is only present within the sensor field-of-view (FOV) in open-air monitoring applications. Fast data acquisition also addresses the rapid change in sensor FOV when mounted on a mobile vehicle.

The data processing steps begin with the application of digital filters to the interferogram segment to furnish spectral selectivity to the interferogram analysis. Proper digital filter design accepts only the modulated interferogram frequencies that are associated with an absorption or emission band of a target vapor analyte. The filtered interferogram segment is converted into a characteristic pattern for the detection of target vapor. Input of the filtered interferogram segment into a numerical pattern recognition algorithm allows the development of an automated procedure for detecting the target vapor analyte.

Previous work employed a single filter, depending solely upon the filter attenuation characteristics to reject the spectral information arising from compounds other than the analyte potentially present in the sensor FOV.[6-10] This approach proved workable, but it was limited in cases for which the vapor analyte information was overwhelmed by a large interference signal. This situation arose, for example, when it was necessary to monitor a minor analyte vapor component in a stack emission that was dominated by a species possessing some spectral overlap with the target vapor analyte.

In this study, a multiple filtering strategy was evaluated for its potential to enhance the selectivity for this type of direct interferogram analysis. Passive FT-IR laboratory and field interferogram data of a mixture of vapors with overlapping spectra were used to test the selectivity of multiple digital filtering. Two protocols were implemented based on the use of (1) a single filter positioned on an analyte band and (2) two filters positioned on one analyte and one interference band. The filtered interferogram segments were subjected to a piecewise linear discriminant analysis for implementing an automated procedure in determination of the target analyte presence with remote sensing measurements. The target vapor analyte in this study was ethanol and the principal interference vapor was ammonia.

2. EXPERIMENTAL PROCEDURE

This study employed two data sets, one collected in the laboratory (data set **A**) and the second collected in the open air (data set **B**). Data set **A** was collected with a Midac Outfielder FT-IR emission spectrometer (Unit 120, Midac Corp., Irvine, CA). The instrument used a liquid nitrogen cooled Hg:Cd:Te detector which was designed to respond over the spectral range of 800 to 1400 cm^{-1}. The data acquisition was performed with a Dell 486P/50 computer (Dell Computer, Austin, TX) and the MIDCOL software package.[12] The maximum spectral frequency was 1974.75 cm^{-1}, with the interferogram data points sampled at every eighth zero crossing of the HeNe reference laser. The interferograms contained 1024 data points, and the point spacing in the corresponding single-beam spectra was nominally 4 cm^{-1}. All interferograms were single scans (i.e., no signal averaging).

The spectrometer was configured to view the IR radiation from a 4 by 4-in. extended blackbody (Model SR-80, CI Systems, Agoura, CA). This source was varied over the range of 5 to 50 °C with an accuracy of ±0.03 °C and precision of ±0.01 °C. A gas cell with 8.2 cm pathlength and low-density polyethylene windows (0.0005-in. thickness) was placed between the source and spectrometer such that the the spectrometer had a unobstructed FOV through the cell. This simulated field data collection experiments in which a target vapor is viewed against a variable background IR radiance. The cell temperature was uncontrolled, but was monitored with a thermistor. Across the data collection experiments, measured cell temperatures ranged from 22 to 26 °C. When the cell temperature was higher than the blackbody background, spectral signals of the target vapor components of the samples were observed as emission bands. Absorption bands were observed for the corresponding cases in which the gas cell temperature was lower than that of the background.

For a given sample concentration, the blackbody temperature was initially set to 50 °C and interferograms were collected with no cell in the optical path, with the empty cell in place, and with the vapor filled cell in the FOV. Fifty interferograms were collected for each of these three conditions. This procedure was repeated at each step as the blackbody temperature was lowered to 45, 40, 35, 30, 29, 28, 27, 26, 25, 24, 23, 22, 21, 20, 15, 10, and 5 °C. The data collection was then completed by raising the temperature to two final settings, which was varied somewhat over the 12 data runs. In eight cases, the final temperatures were 25.5 and 50 °C. The other combinations were 18/32, 18/31, 24.5/25.5, and 18/50 °C. The data runs were performed in two blocks. Eight runs over 22 days were performed in the first block, and four runs over four days comprised the second block. The blocks were separated by 167 days. These time spans resulted as expected in some instrument drift that is reflected in the collected data.

The target vapors were generated by vapor liquid equilibration of various aqueous solution concentrations (i.e., dilutions) of absolute ethanol (AAPER Alcohol and Chemical Co., Shelbyville, KY), acetone (Aldrich Chemical Co., Madison, WI, 99.5+%), ammonium hydroxide (Aldrich, ACS Reagent Grade) and mixtures of acetone/ethanol, ethanol/ammonium hydroxide, and acetone/ammonium hydroxide. The ternary aqueous mixtures were used to simulate conditions in which the analyte (i.e, solute), ethanol, must be detected in the presence of an interfering vapor constituent (e.g., acetone or ammonia). Twelve data runs were made consisting of nine different dilution factors and three duplicate runs. Table 1 describes the data runs performed.

Estimated solution concentrations depended upon the tabulated densities to compute mole fractions.[13,14] The Wilson and Antoine equations were subsequently employed to compute activity coefficients and pure substance vapor pressures, respectively.[15,16] These combined values permitted estimation of the target vapor partial pressure above the aqueous solutions. These solute vapor partial pressures and cell pathlength allowed the computation of the path averaged concentrations for the particular sample components. Units of parts per million-meter (ppm-m) were used for comparison with field remote sensing experiments in which the sample resided in an open-air environment over an uncontrolled pathlength. As presented in Table 1, the estimated concentration ranges for ethanol, ammonia, and acetone were 150-700, 100-450, and 950-3700 ppm-m, respectively.

Table 1. Estimated CLs for Laboratory Aqueous Solutions of Data Set A

Run	Sample composition (dilution factors)	Cell temp. (°C)	[Ammonia][a] (ppm-m)	[Ethanol][a] (ppm-m)	[Acetone][a] (ppm-m)
1	1/32 ethanol	24.7 - 25.0		341 - 347	
2	1/64 ammonia	23.9 - 24.9	101 - 104		
3	1/64 acetone	24.8 - 25.7			963 - 1001
4	1/16 acetone + 1/16 ethanol	24.2 - 25.2		626 - 664	3446 - 3598
5	1/32 ammonia + 1/16 ethanol[b]	24.9 - 26.1	218 - 226	652 - 699	
6	1/32 ammonia + 1/16 ethanol[b]	25.3 - 26.2	220 - 227	667 - 703	
7	1/16 ammonia + 1/64 ethanol[b]	22.2 - 22.4	439 - 442	152 - 153	
8	1/16 ammonia + 1/64 ethanol[b]	23.3 - 23.8	455 - 462	161 - 166	
9	1/16 ammonia + 1/16 ethanol[b]	22.1 - 22.3	438 - 455	553 - 594	
10	1/16 ammonia + 1/16 ethanol[b]	22.6 - 22.9	445 - 449	570 - 580	
11	1/32 ammonia + 1/16 acetone	25.1 - 25.6	219 - 222		3583 - 3660
12	1/64 ammonia + 1/16 acetone	25.2 - 25.7	105 - 106		3598 - 3676

[a]Estimated path-averaged concentration based on computed vapor pressures. Range denotes minimum and maximum concentrations computed from the minimum and maximum cell temperatures measured across the data collection.

[b]Conditions run in duplicate.

Data set **B** was collected with a Brunswick FT-IR emission spectrometer (Unit 21, Brunswick Technical Group, DeLand, FL), which incorporated a Hg:Cd:Te detector with a Magnovox closed-cycle Stirling cooler. The FOV of the instrument was controlled with an antireflection-coated germanium refractive optic telescope (Intellitec, DeLand, FL), which restricted the sensor FOV to 0.5°. The MIDAS software package was used in the data acquisition.[17] The interferogram sampling parameters described previously for the data collected with the Midac instrument were again used. Single-scan interferograms were collected as described previously.

For this data set, analyte plumes were generated from a stack 4.5 m in height and with a exit diameter of 0.4 m (Aerosurvey, Inc., Manhattan, KS). Details of the plume generation were presented previously,[18] and only information important to the current work is considered. The stack output temperatures ranged from approximately 125 to 300 °C. The data used in this study were compiled from two 4-day field experiments separated by 131 days (August 1997 and December 1997). In both open-air experiments, the spectrometer monitored the stack from ground level. The distance from the spectrometer to the stack was approximately 50 m for the first open-air experiment and 200 m for the second open-air experiment. The stack emission was viewed against a low angle sky spectral background. Spectral features of the released target vapors were observed exclusively as emission bands, due to the infrared radiance differential between elevated temperature vapor plume and low temperature sky background.

Pure ethanol (AAPER Alcohol and Chemical Co.) and anhydrous ammonia (99.99%, Matheson Gas Products, Joliet, IL) and mixtures of ethanol/ammonia were released from the plume vapor generator. In addition, several releases of pure sulfur hexafluoride (99.8%, Matheson Gas Products) and methanol (AAPER Alcohol and Chemical Co.) were performed. The methodology for estimating analyte concentrations relied on the use of flow tubes, which were calibrated gravimetrically for each chemical species released. Linear calibrations of the five flow tubes used were based on one to four mass flux measurements for each vapor analyte. This allowed the emission rate of each compound to be estimated for a given flow tube setting. By assuming the released compounds were completely vaporized and behaved as ideal gases, emission rates were converted to volume flow rates by use of the ideal gas law. Concentrations were then estimated by dividing the volume flow rates of the released compounds by the overall volumetric air flow rate of the stack. Air flow rates were computed from the differential pressures measured across the two ports of a Pitot tube placed in the center of the stack. Path-averaged concentrations in ppm-m were computed by estimating the optical path length of the measurement as 0.4 m, the diameter of the stack.

In addition to data collected during the stack vapor generated plumes, separate spectral measurements were made each day of various sky, terrain, and horizon backgrounds. Backgrounds also included the spectral measurements directly above the elevated temperature stack when no vapors were being released. A 12 by 12-in. extended blackbody source (Model 140; Graseby Infrared Systems, Orlando, FL) was also positioned to fill the FOV of the spectrometer periodically allowing collection of reference blackbody spectral data at known temperatures.

These experiments produced 38 data runs corresponding to 14 ethanol releases and 24 runs in which another interference vapor was released or background interferograms were

collected. Six of the runs included mixtures releases of ethanol and ammonia. Estimated concentration ranges for the pure vapor components and ethanol/ammonia mixture releases ranged from 0-4800 and 0-1500 ppm-m, respectively. Tables 2 and 3 summarize the open-air spectral data collected.

The collected interferograms comprising laboratory and open-air experimental data sets were transferred to Silicon Graphics Indigo-2 IMPACT 10000 workstations (Silicon Graphics, Mountain View, CA) operating under Irix (version 6.2). All computations were performed on these workstations using original software written in FORTRAN 77. Some computations used subroutines from the IMSL library (IMSL, Houston, TX).

3. RESULTS AND DISCUSSION

3.1 Characterization of Spectral Data.

Vapor-phase library spectra with a nominal point spacing of 2 cm^{-1} are presented in Figure 1 for pure (A) ethanol, (B) ammonia, and (C) acetone. These spectra are taken from the Nicolet-Aldrich vapor phase library. The ethanol C-O stretching band is selected as the target band for the automated detection algorithm devised in this study. The center of mass of this band is 1058 cm^{-1}, and the peak maximum coincides with the location of the *Q* branch at approximately 1066 cm^{-1}. Comparison of the spectra of the three compounds reveals that the principal spectral interference for the targeted ethanol band arises from the rotational fine structure spectra of ammonia. These are the antisymmetric and symmetric H-N-H deformation bands of ammonia with centers of mass at 964 and 929 cm^{-1}, respectively.

The effect of spectral overlap is clearly visible in Figure 2. Absorbance spectra of mixture samples are plotted in Figure 2 that are computed from interferograms in Data set **A**. The background blackbody temperature is 50 °C in each case. The interferograms are Fourier transformed into single-beam spectra with triangular apodization, Mertz phase correction, and one level of zero-filling. A 128-point symmetric interferogram is used in calculating the phase spectrum. The nominal spectral point spacing is 2 cm^{-1}, the same as in Figure 1. The transmittance values are obtained by ratioing the passive single-beam spectrum of the target vapor in the gas cell to a similarly processed passive single-beam spectrum of the empty blank cell. These transmittance values are converted to absorbance units and are displayed in Figure 2. In calculating these passive absorbance values, no correction is made for the self-emission of the optical system.[19]

The ethanol C-O band in Figure 2A is seen to be relatively free of overlap from the acetone C-CO-C backbone stretching band with center of mass at 1214 cm^{-1}. The spectral overlap of the targeted ethanol band with the rotational structure of the ammonia bands is illustrated by Figures 2B and 2C. As the ammonia concentration is increased relative to that of ethanol (Figure 2C), the ethanol absorption is increasingly obscured by the ammonia spectral features. This simulates a monitoring scenario in which ethanol is to be detected as a minor component of a stack effluent. This study evaluates the degree that digital filtering and pattern recognition strategies isolate the ethanol information from the various background signatures.

Table 2. Experimental Conditions of Data Set B for Ethanol-Active Data

Run	Expt.[a]	Day	Stack Temp. (°C)	Chemical Composition	Training	Pred. I
1	1	1	198-204	229-1629 ppm-m ethanol	2136	12418
2	1	1	171-178	1555-1587 ppm-m ethanol	689	4751
3	1	3	249-251	643-644 ppm-m ethanol	609	2300
4	1	3	198-201	628-653 ppm-m ethanol	428	2572
5	1	3	173-176	644-677 ppm-m ethanol	148	2852
6	1	3	118-129	1400-1518 ppm-m ethanol	116	2075
7	1	4	196-203	52-522 ppm-m ethanol/163-176 ppm-m ammonia mixtures	49	2023
8	1	4	173-177	405-496 ppm-m ethanol/175-181 ppm-m ammonia mixtures	61	2139
9[b]	1	4	171-178	0-405 ppm-m ethanol/170-183 ppm-m ammonia mixtures	0	0
10	1	4	196-200	Variable ethanol and ammonia mixtures	11	126
11	1	4	192-201	2325-2481 ppm-m ethanol/7-69 ppm-m ammonia mixtures	276	6124
12	1	4	174-177	2345-4808 ppm-m ethanol/10-63 ppm-m ammonia mixtures	477	4522
13	2	2	189-208	739-3125 ppm-m ethanol	872	4619
14	2	2	173-177	2061-2571 ppm-m ethanol	2128	3381

[a]Indicates the first or second open-air experiment.

[b]Run 9 was withheld to form Prediction Set **II**.

Table 3. Experimental Conditions of Data Set B for Ethanol-Inactive Data

Run	Expt.[a]	Day	Stack Temp. (°C)	Chemical Composition	Training	Pred. I
15	1	1	-	Blackbody and sky backgrounds including sky above heated stack	266	7256
16	1	1	214	29 ppm-m sulfur hexafluoride	5	1206
17	1	1	202-206	97-402 ppm-m methanol	270	7802
18	1	1	174-175	383-402 ppm-m methanol	220	4757
19	1	1	-	Blackbody (37-80 EC)	39	1813
20	1	2	196-206	94-416 ppm-m ammonia	70	8030
21	1	2	175-176	390-403 ppm-m ammonia	75	8462
22	1	2	191-202	7-280 ppm-m ammonia	90	16410
23	1	2	-	Sky backgrounds above heated stack; some methanol and ammonia	180	9559
24	1	2	195-204	308-1381 ppm-m methanol	219	5781
25	1	2	172-177	661-1386 ppm-m methanol	630	5370
26	1	2	-	Blackbody (ambient to 80 °C)	436	1684
27	1	3	-	Sky backgrounds above heated stack; some ammonia and sulfur hexafluoride	705	16139
28	1	3	174-205	475-1039 ppm-m ammonia	683	8317
29	1	3	-	Sky backgrounds above heated stack; horizon and tree backgrounds	262	14438
30	1	3	-	Blackbody (ambient to 80 °C)	50	3260
31	1	4	-	Sky, terrain, and horizon backgrounds	93	4510
32	1	4	-	Blackbody (ambient to 70 °C)	280	2420
33	1	4	191-208	7-67 ppm-m ammonia	427	11573
34	2	1	-	Sky backgrounds above heated stack	398	2601
35	2	1	202-206	456-1519 ppm-m ammonia	953	6944
36	2	1	173-175	898-1258 ppm-m ammonia	253	3001
37	2	3	301-306	692-991 ppm-m ammonia	404	4175
38	2	4	301-305	852-1036 ppm-m ammonia	992	4600

[a]Indicates the first or second open-air experiment.

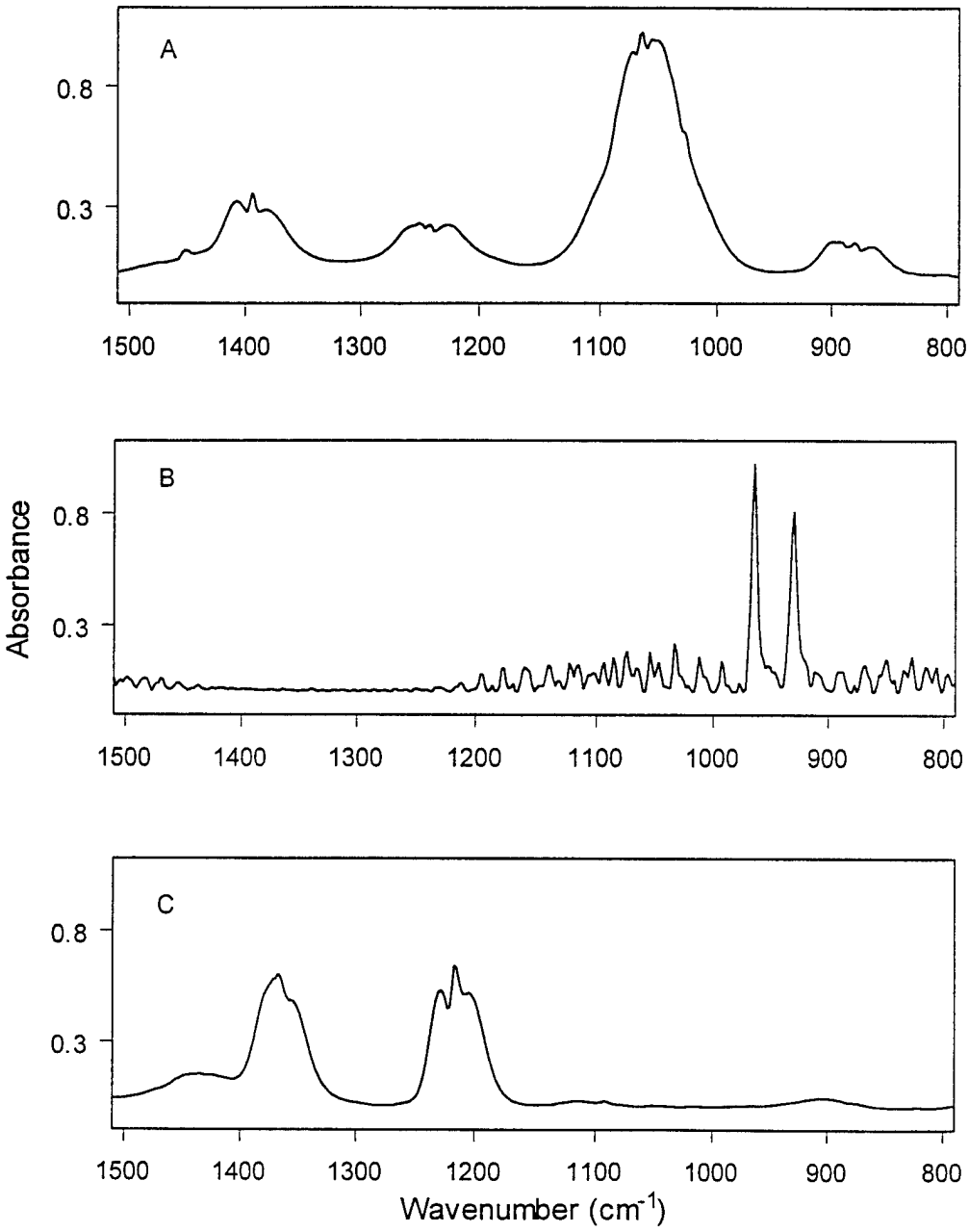

Figure 1. **Library Vapor-Phase Absorbance Spectra of (A) Ethanol, (B) Ammonia, and (C) Acetone**

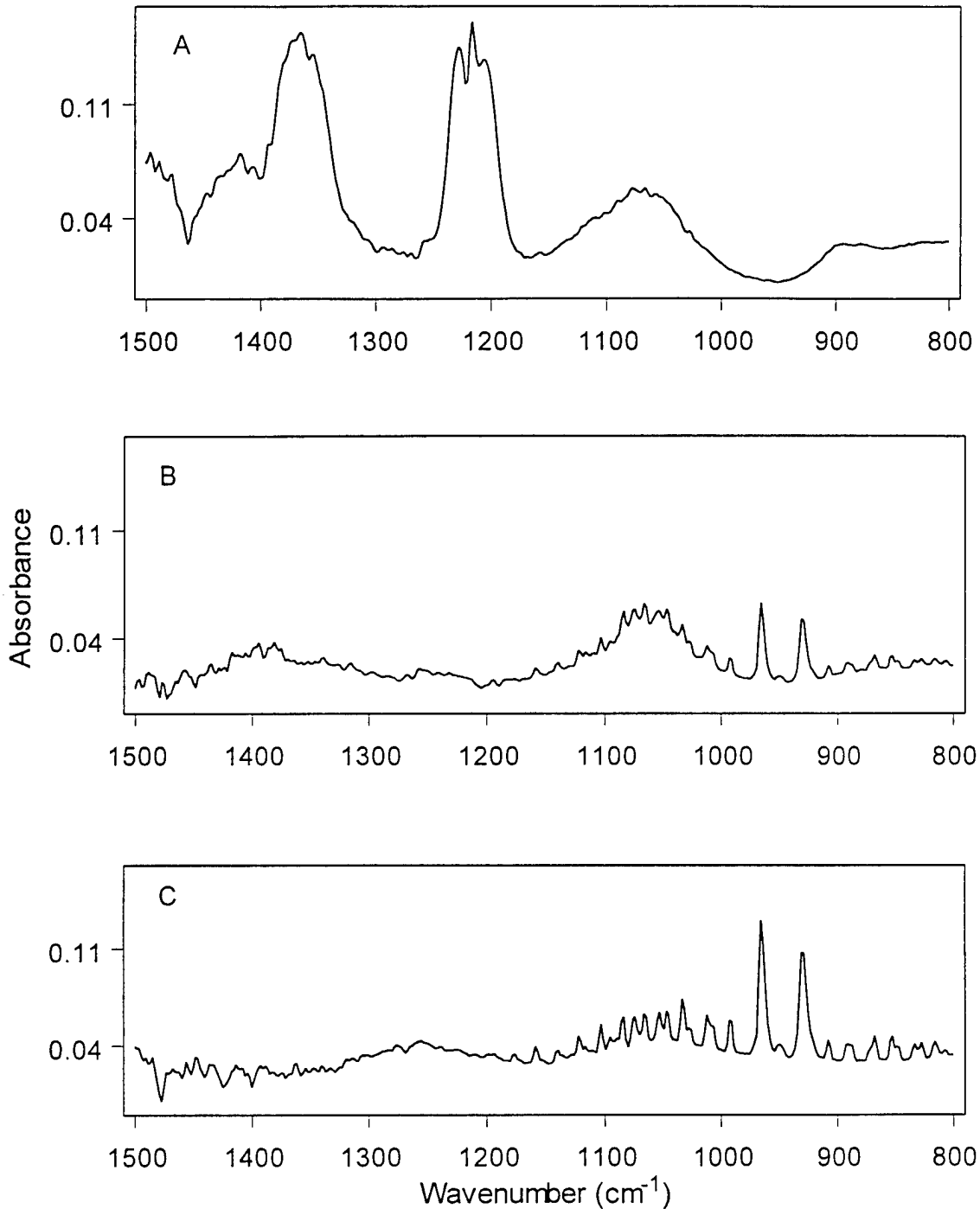

Figure 2. **Passive Absorbance Spectra from Data Set A with Aqueous Dilution Factors, Estimated CLs of (A) 1/16 Acetone, 3346-3598 ppm-m + 1/16 Ethanol, 626-664 ppm-m; (B) 1/32 Ammonia, 218-226 ppm-m + 1/16 Ethanol, 652-699 ppm-m; and (C) 1/16 Ammonia, 455-462 ppm-m + 1/64 Ethanol, 161-166 ppm-m**

3.2 Overview of Data Analysis Methodology.

The data analysis methods are based on the isolation of the vapor analyte signature directly from the sampled interferogram data. Interferograms are preprocessed by a two-step procedure. First, a four-term high-pass filter is applied to remove low-frequency noise. Second, the filtered interferogram is normalized in the vector sense to unit length. Frequency selectivity for the target vapor analyte is achieved by applying one or more bandpass digital filters to the preprocessed interferogram for extracting the modulated frequencies corresponding to a spectral band of either an analyte or interference spectral feature. Further selectivity using band width is accomplished by selecting the proper interferogram segment that is displaced from the interferogram ZPD. The frequency position and width of the filter bandpass, as well as the starting and ending points of the interferogram segment, represent the optimization variables.

The digital filtering methodology focuses on time-varying finite impulse response (FIR) filters. The filter coefficients are derived from interferogram data by use of a multiple linear regression procedure.[20] Table 4 lists the specifications for the filters that are used with data set **A**. The table includes the position of the filter passband, the width-at-half-maximum of the passband, and the average attenuation (in dB) in the filter stopbands. Three ethanol and nine ammonia filter specifications are considered in this investigation.

The use of either one filter positioned on the ethanol C-O band or a combination of two filters, one positioned on the ethanol band and one positioned to extract information about the ammonia interference are explored. When two filters are used, each filter is applied to a specific segment of the preprocessed interferogram. The two resulting filtered segments are concatenated for use in subsequent calculations.

To automate the detection of ethanol, the filtered interferogram segments are supplied as the input vectors to piecewise linear discriminant analysis (PLDA).[21,22] The PLDA is a numerical pattern recognition method that is based on the calculation of multiple linear boundaries (termed "discriminants") dividing the input data space into regions corresponding to user-defined categories. The boundary is a hyperplane and is mathematically defined by its normal vector. Positioning this vector in this study is accomplished by a simplex optimization procedure, although other numerical optimization methods are possible.[23] A training set of example patterns is used to locate the discriminants. Unknown patterns are subsequently classified by their position with respect to the computed training set boundary (i.e., on which side of the boundary they lie). A calculated discriminant score indicates the distance of a pattern from the boundary, with positive scores indicating a location on the analyte-active side of the boundary.

In the present application, two data categories exist, corresponding to the presence or absence of the target analyte ethanol. The PLDA method assumes that the input vectors with characteristic signatures cluster in the data space in a way relating to their particular category. For the passive remote sensing application, this requires the ethanol signature to be evident in the filtered interferogram, regardless of presence or absence of ammonia or acetone spectral interferences.

Table 4. Digital Filter Parameters for Data Set A

Filter	Position[a] (cm^{-1})	Width[b] (cm^{-1})	Attenuation[c] (dB)
Ethanol Filters			
1	1068	120	28.4
2	1068	135	27.5
3	1068	147	26.6
Ammonia Filters			
4	930	104	28.1
5	930	116	28.1
6	930	135	26.9
7	957	108	28.5
8	957	120	28.3
9	957	143	27.2
10	945	104	28.0
11	945	120	28.0
12	937	139	27.1

[a]Location of minimum attenutation in the filter passband.

[b]Width at half-maximum of the filter passband.

[c]Average attenuation in the stopband computed over the range of 400 to 700 cm^{-1}.

Multiple discriminants provide an approximation to a nonlinear boundary between data categories. In the present implementation of PLDA, this is accomplished by computing the individual discriminants in a stepwise manner. Each discriminant is optimized to separate as many analyte-active training patterns as possible, by defining a "pure" side of the boundary that contains only patterns in the analyte-active class. Once separated, these analyte-active patterns are removed from further consideration. The next discriminant is computed from the remaining "mixed-class" group of patterns. This process continues until one of two conditions exist. Condition one is that all analyte-active patterns have been separated. Condition two is that the remaining patterns in the mixed-class group are indistinguishable (i.e., further separation of analyte-active patterns is not possible). In the current effort, complete separation is achieved in several cases with data set **B**, but is never achieved with data set **A**. For the cases in which complete separation is not achieved, individual discriminants are computed until no additional patterns in the training set are separated or until a maximum of five discriminants is reached.

Table 5. Partitioning of Data Sets A and B

Data category	Training set	Prediction set[a]
Data set **A**		
Analyte-active	4800	3200
Analyte-inactive	8300	18400
Data set **B**		
Analyte-active	8000	49902
Analyte-inactive	8000	160108

[a]Prediction set **I** for data set **B** is described.

3.3 Analysis of Data Set A.

The collected interferograms were subdivided into training and prediction sets for optimizing and testing the digital filtering/pattern recognition methodology. As discussed previously and indicated in Table 1, 12 individual laboratory data runs were employed based on nine sample compositions. Each data run included 20 groups of 150 interferograms corresponding to 20 temperature settings of the background extended blackbody source. Within each group, 50 interferograms each were acquired for three conditions of (1) the vapor filled cell, (2) blank empty cell, and (3) no cell intervening between sensor/blackbody. Different procedures were used for assigning interferograms to the training and prediction sets in the ethanol-active and ethanol-inactive data categories.

For the ethanol-active category, a *sample* in a data run was defined as the combination of an ambient vapor composition and blackbody background temperature. Samples were assigned in an alternating manner to the training and prediction sets. For the first 18 blackbody background temperature settings in each run, the training set contained blackbody temperatures of 50, 40, 35, 29, 27, 25, 24, 23, 21, 10, and 5 °C, where as the prediction set contained blackbody temperatures of 45, 30, 28, 26, 22, 20, and 15 °C. As noted previously, the 19^{th} and 20^{th} temperature settings varied from run to run and were assigned to the prediction and training

sets, respectively. In each case, the 50 replicate interferograms corresponding to a *sample* were carried together into either the training or prediction set.

The ethanol-inactive category contained three types of interferogram scans: (1) blank empty cell, (2) blackbody without the intervening cell present, and (3) cell containing combinations of acetone/ammonia interference vapor mixtures. Interferogram scans of the empty cell and blackbody backgrounds only at all temperatures were assigned to the training and prediction sets using the subset selection algorithm developed by Carpenter and Small.[24] For interferogram scans of the filled vapor cell containing acetone, ammonia, and acetone/ammonia mixtures, interferograms were assigned to the training and prediction sets by use of the same alternating blackbody temperature procedure described previously for the ethanol-active category. Also as before, the 50 replicate interferograms in each experimental condition were grouped into the training or prediction sets. The resultant number of interferograms that are assigned to either the training or prediction sets for each data category are given in Table 4.

An optimization procedure was used to identify the optimal digital filtering and interferogram segment parameters for use with the PLDA algorithm. Three general strategies were employed in implementing the ethanol detection: (1) use of a single ethanol filter and a 60-point segment of the interferogram, (2) use of a single ethanol filter and a 120-point interferogram segment, and (3) use of one ethanol and one ammonia filter applied to individually optimized 60-point interferogram segments, with the resulting filtered points concatenated to form a 120-point segment. Selection of 120 points as the maximum segment length was based on a previous study.[10]

With each of the three strategies described above, a grid search optimization was performed to determine the optimal filter(s) and corresponding interferogram segment location(s). The three ethanol filters listed in Table 4 were first evaluated in conjunction with 60 and 120-point interferogram segments. With each filter, the segment starting position was varied from points 25 to 175 for increments of 25 points. The ZPD point was defined as point 1. For each combination of filter and segment, PLDA was applied to the training set. Each computed piecewise linear discriminant consisted of 3 to 5 individual discriminants. In each case, the discriminant optimization was terminated when no additional ethanol patterns were reliably separated. The resulting discriminants were ranked on the basis of the total number of training patterns correctly classified. For each of the three filters, the interferogram segment that produced the optimal results was selected, and the corresponding discriminant was used to classify the patterns in the prediction set.

Table 6 lists the classification performance of each discriminant when applied to the training and prediction sets. Training results are listed for only ethanol detections because the PLDA algorithm discriminants separate ethanol-active patterns from the current mixed subset of ethanol-active and ethanol-inactive patterns. Thus, ethanol-inactive patterns in the training set are never misclassified. For the prediction set, correct ethanol detections are tabulated along with false detections (i.e., false positives). The total number of correct classifications in the prediction set is also listed.

The two-filter approach was implemented by finding the best ammonia filter and corresponding interferogram segment, then adding it to each of the optimal ethanol filter/60-

Table 6. Pattern Recognition Results for Laboratory Data Set A

Filter(s) used[a]	Segment[b]	Correct ethanol detections (training)	Correct ethanol detections (prediction)	False ethanol detections (prediction)	Total correct classifications (prediction)
Ethanol filter and 60-point segment					
1	51-110	3528 (73.5%)	2421 (75.7 %)	74 (0.4 %)	20747 (96.1 %)
2	51-110	3514 (73.2 %)	2214 (69.2 %)	69 (0.4 %)	20545 (95.1 %)
3	51-110	3490 (72.7 %)	2204 (68.9 %)	28 (0.2 %)	20576 (95.3%)
Ethanol filter and 120-point segment					
1	26-145	3817 (79.5%)	2481 (77.5%)	40 (0.2%)	20841 (96.5%)
2	51-170	3766 (78.5%)	2507 (78.3%)	109 (0.6%)	20798 (96.3%)
3	26-145	3690 (76.9%)	2478 (77.4%)	119 (0.7%)	20759 (96.1%)
Ethanol and ammonia filters with total segment of 120 points					
2 10	51-110 26-85	4074 (84.9%)	2819 (88.1%)	87 (0.5%)	21132 (97.8%)
3 12	51-110 26-85	4046 (84.3%)	2656 (83.0%)	95 (0.5%)	20961 (97.0%)
1 8	51-110 51-110	3982 (83.0%)	2695 (84.2%)	29 (0.1%)	21066 (97.5%)

[a]Refers to filter numbers in Table III.

[b]Starting and ending interferogram points where point of ZPD = 1.

point segment combinations listed in Table 6. For each of the ammonia filters listed in Table 4, a grid search was performed to identify the best 60-point segment to use with each ethanol filter/segment. Starting points for the ammonia segments were investigated over the range of points 25 to 150 in steps of 25 interferogram points. As noted previously, the ethanol and ammonia filters were applied separately to the same preprocessed interferogram data, and the resulting filtered segments were concatenated. For each 120-point concatenated segment, piecewise linear discriminants were computed as described previously by use of the training set. The best combinations were selected on the basis of the number of training patterns correctly classified. The corresponding discriminants were then applied to the prediction set. Training and prediction results are given in Table 6 for the best ammonia filter/segment combinations that were found for use with the previously optimized ethanol filter/segment combinations. The corresponding piecewise linear discriminants contained either 4 or 5 individual discriminants. Inspection of Table 6 reveals that the results among the three detection strategies differ primarily in their ability to make positive ethanol detections. False detections are 0.7% or less in all cases. Focusing on correct ethanol detections in the prediction set, the general trend in the results is greater ethanol detection sensitivity (i.e., higher ethanol classification percentages) for the two-filter strategy versus either of the single-filter approaches. In the best cases in which a single filter was used, increasing the ethanol segment from 60 to 120 points improves the detection percentage from approximately 76 to 78%. Adopting the two-filter approach increases the ethanol detection percentage to 88%.

A two-sample *t*-test was also used to establish a statistical basis for comparing the results in Table 6. The three classification results for the application of each method to the prediction set were used to define the samples for comparison. A one-tailed test was used for each comparison along with separate variance estimates. The ethanol detection percentages for the two-filter approach were found to be greater than those for the 60-point and 120-point single-filter methods at probabilities of 0.007 and 0.02, respectively. A similar comparison of the false detection percentages found no statistically significant improvement afforded by the two-filter approach.

Further understanding of the prediction results requires knowledge of the signal strengths in the spectral data. The differential temperature between the gas cell contents and blackbody source impacts these signal strengths, as well as the vapor concentration and pathlength. The signal detected by a passive IR remote sensor at a speicific wavenumber is given by equation 1.

$$P = [T_a T_t N_b + (1 - T_a T_t) N_t] B \qquad (1)$$

The P denotes the power of the light incident on the sensor; T_a represents the transmittance of the intervening atmosphere between the IR background and the sensor; T_t indicates the transmittance of the target vapor sample in the FOV of the sensor; N_b signifies the spectral radiance of the background; N_t denotes the radiance of a blackbody at the same temperature as the vapor sample; and B is a parameter related to the optical collection efficiency of the sensor.[25] For a concentration range over which the Beer-Lambert law holds, T_t in equation 1 is expressed as $e^{-\Sigma acl}$, where the summation contains a contribution from each chemical constituent of the vapor sample. For each species, a denotes the absorptivity, c represents the concentration, and l signifies the optical pathlength of the target vapor sample. The $T_a T_t N_b$ term describes the

absorption of background IR energy by the vapor sample constituents, whereas the $(1 - T_a T_t)N_t$ term describes the self emission of IR energy from these vapor species.

An inspection of equation 1 reveals that the net signal arising from the chemical constituents of the vapor sample depends on the difference between N_b and N_t. For example, if $N_t = N_b$, then equation 1 reduces to $P = N_t B$. This illustrates the situation in which absorption and emission occur at the same rate. Thus, this condition results in no detectable spectral signals from the target vapor sample. This shows the inherent limitation of the passive remote sensing measurements, which depend on the existence of a sufficient radiance differential between the vapor sample and background scene. The radiance levels, as described by the Planck function, are determined by the temperature of the extended blackbody source. In practice, passive IR detection of a vapor target analyte relies on three factors: (1) a sufficiently large product of *acl* for the vapor analyte, (2) a sufficiently small $\sum acl$ for the other chemical species present, and (3) a sufficiently large temperature differential between the vapor sample and the background.

On the basis of the preceeding theoretical treatment, the signal strengths of the passive data are evaluated by visual inspection of the spectra computed from the collected interferogram data as a function of the temperature differential between the vapor cell contents and blackbody source. Because the Fourier transform is a linear operation, the signal strengths present in the interferogram domain are then be assumed to be analogous.

To evaluate the signal strengths of the prediction data, spectral signal-to-noise (S/N) ratios were computed as a function of the temperature differentials. Single-solute component runs of ethanol, ammonia, and acetone at the same aqueous dilution factors present in the prediction set were used in these comparisons. Transmittance spectra were calculated by ratioing single-beam spectra of the vapor containing cell to the corresponding single-beam spectra of the blank empty cell. The resultant transmittance spectra were converted into spectral absorbance units. The single-beam spectra were obtained by Fourier transforming the associated interferograms with triangular apodization and Mertz phase correction.

To calculate root-mean-square (RMS) noise values in the regions of the spectral bands, difference spectra were obtained by subtracting absorbance spectra computed from consecutive single scans. The noise in a difference spectrum, s_d, was determined by a least-squares fitting over a 100 cm^{-1} spectral region to a linear baseline and subsequently computing the RMS noise about this fitted line. By the principles of error propagation, the noise in the original absorbance spectra, s_a, was found with equations 2 and 3.

$$s_a \cdot s_d / 2^{1/2} \tag{2}$$

$$s_d = [s_1^2 + s_2^2]^{1/2} \cdot 2^{1/2} s_a \tag{3}$$

The noise levels were represented by s_1 and s_2 in the first and second replicate absorbance spectra, respectively. Each of these levels are assumed to be equal to s_a. The spectral wavenumber ranges for computing the noise levels of the ethanol, ammonia, and acetone absorbance data were 1000-1100, 900-1000, and 1165-1265 cm^{-1}, respectively. These spectral peak regions contained the principal spectral bands that influenced the ethanol determination.

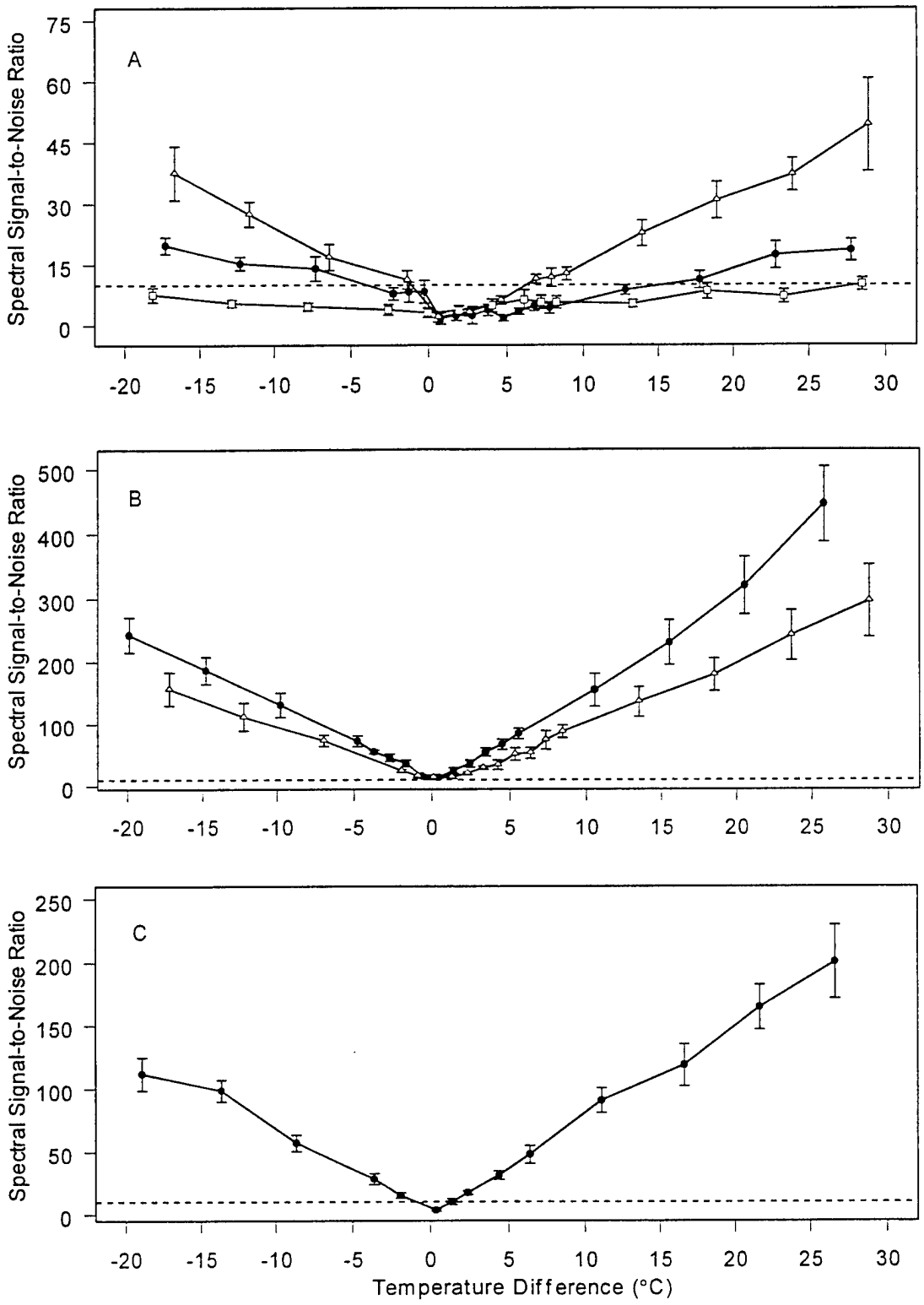

Figure 3. **Spectral Signal-to-Noise Ratios (S/N) as a Function of the Differential Temperature for (A) Three Ethanol Dilution Factors, Estimated CL Values; (B) Two Ammonia Dilution Factors, Estimated CL Values; and (C) One Acetone Dilution Factor, Estimated CL Value**

Calculation of the S/N values was based on determining the maximum absorbance value at the spectral peak regions noted previously, averaged across each pair of replicate absorbance spectra considered. The resulting peak absorbance was ratioed to the estimated noise level to obtain the S/N value. A complicating factor at low signal levels was the presence of interference fringes in the spectra arising from the thin polyethylene gas cell windows. These fringes were suppressed by use of a digital Fourier filter prior to the calculation of the peak maximum. Following the filtering step, a second order polynomial baseline was computed by use of the two 50 cm^{-1} regions on each side of the spectral peak regions. The baseline contribution was subtracted from the peak maximum by use of this model before the S/N value was computed.
At each blackbody temperature, eight pairs of replicate absorbance spectra are determined, and the average S/N values are computed by relying on the computational methodology previously described. For each solution sample composition (i.e., dilution factor) that occurs in the prediction set, Figure 3 plots the computed spectral S/N values as a function of the temperature differential between the blackbody and cell contents. Positive temperature differences correspond to the case in which the blackbody is at a higher temperature than the gas cell contents (i.e., the vapor analyte spectral features are present as absorption bands). Negative temperature differences represent the case in which the blackbody is at a lower temperature than the gas cell contents (i.e., the vapor analyte spectral features are present as emission bands). However, the values in Figure 3 are plotted in absorbance units, which by definition are always positive. Plots of the absorbance values are provided for the target analytes of (A) ethanol, (B) ammonia, and (C) acetone in Figure 3. The error bars are plotted for each temperature at the 95% confidence interval about the mean of the eight computed S/N values. The three ethanol dilution factors and estimated path-averaged concentrations are represented in Figure 3A by open triangles for 1/16, 521-540 ppm-m; solid circles for 1/32, 294-296 ppm-m; and open boxes for 1/64, 145-162 ppm-m. The two ammonia dilution factors and estimated path-averaged conentrations are denoted in Figure 3B by solid circles for 1/16, 468-479 ppm-m and open triangles for 1/32, 194-204 ppm-m. The one acetone dilution factor and estimated path-averaged concentration are shown in Figure 3C by solid circles for 1/16, 3314-3402 ppm-m. The horizontal dashed line in each plot of Figure 3 is drawn at S/N = 10.0, which corresponds to the conventional definition of the limit of quantitation (LOQ).[26] The signal level corresponding to the LOQ is often taken as the smallest useable signal for the purpose of implementing an analytical determination.

As described by equation 1, the general trend in the plots of Figure 3 is a decrease in S/N as the temperature differential approaches zero. An increase in concentration causes the S/N values to shift in a positive direction, but similar behavior with respect to temperature is observed for each concentration. Comparison of the data across the three compounds reveals that the ammonia and acetone S/N values greatly exceed those of ethanol. It is important to note that the ethanol S/N values in much of the prediction data lie below the LOQ cutoff.

This assessment of the relative signal strengths of ethanol, ammonia, and acetone vapor components provides some context for the relatively low ethanol detection percentages of 76 to 88% reported previously in Table 6. Further insight into these results is obtained by an inspection of Table 7. For each of the eight data runs in the prediction set, classification percentages for the ethanol-active interferograms are presented as a function of the absolute temperature differential between the blackbody and sample cell contents. Absorption and

Table 7. Ethanol Prediction Results as a Function of Differential Radiance Temperature for Data Set A

Run[a]	Temperature Differential (°C)					
	0-1	1-2	2-3	3-4	4-5	>5
1	0[b] 0[c] 0[d]	0 42 64	10 27 53	90 96 80	2 2 98	100 100 80
4	0 0 0	0 0 0	1 1 3	0 10 94	30 39 92	96 94.7 100
5	6 3 32	100 100 100	100 100 100	100 100 100	100 100 100	100 100 100
6	0 0 0	62 100 100	100 100 100	100 100 100	100 100 100	100 100 100
7	26 48 58	0 0 0	72 4 82	100 100 100	100 100 100	100 100 100
8	0 0 0	60 20 96	100 100 100	100 100 100	100 100 100	100 100 100
9	2 0 84	0 0 0	68 100 100	100 100 100	100 100 100	100 100 100
10	8 30 82	0 0 0	98 88 100	72 100 100	100 100 100	100 100 100

[a]Run number from Table I.

[b]Ethanol detection percentage based on single ethanol filter and 60-point interferogram segment.

[c]Ethanol detection percentage based on single ethanol filter and 120-point interferogram segment.

[d]Ethanol detection percentage based on ethanol and ammonia filters and total interferogram segment length of 120 points.

emission data are not differentiated in this presentation. The top, middle, and bottom entries, respectively, in each box of the table correspond to the ethanol detection percentage for the cases of a single ethanol filter and 60-point segment; a single ethanol filter and 120-point segment; and ethanol and ammonia filters with a 120-point total segment length. Run numbers refer to the sample composition data in Table 1.

The classification results presented in Table 7 clearly illustrate that the two-filter strategy provides results superior to those produced by either of the single-filter strategies when the detection becomes difficult. In Table 7, detections are made for 16 of the 24 cases with a < 3 °C temperature differential. The two-filter strategy produces the best result in 10 of these cases, and ties for the best result in the other 6 cases. As is expected, the greatest improvement occurs in runs 7-10, where the interfering ammonia species is at its highest concentration of approximately 450 ppm-m.

When the temperature difference was > 3 °C, detections were made in every case. The two-filter strategy achieved or tied the best result in 22 of the 24 cases, although each method was observed to work equally well. The effect of the ethanol S/N values in Figure 3 is clearly evident, as the classification results were observed to improve greatly when the temperature difference was at least 3 °C.

3.4 Analysis of Data Set B.

Data set **B** was used to confirm the applicability of the two-filter strategy for field remote sensing data of stack emissions. The data described in Table 2 were assembled into a training set and two prediction sets (**I** and **II**). The 6000 interferograms comprising Run 9 in Table 2 were first set aside to form prediction set **II**. This data run consisted of a series of ethanol/ammonia mixtures in which the ethanol concentration was decreased incrementally from 405 to 0 ppm-m in the presence of an ammonia concentration that remained approximately constant within the range of 170-183 ppm-m. The 6000 interferograms represent a set of data collected contiguously in time as the releases were performed.

The training set and prediction set **I** were then assembled from the remaining 37 runs described in Tables 2 and 3. To allow an accurate assessment of the training and prediction performance obtained with the data, it was necessary to assign each interferogram with confidence to either the ethanol-active or ethanol-inactive data categories. Separate procedures were used for each category.

The ethanol-inactive data were assembled from runs in which ammonia, sulfur hexafluoride, or methanol were released. Ethanol-inactive data also included blackbody reference measurements and runs measuring various sky, terrain, and horizon backgrounds in the absence of target vapors. In terms of spectral features that could have bearing on the ethanol detection, sulfur hexafluoride possessed a narrow band with center of mass at 942 cm^{-1}, whereas methanol has a band with *PQR* band shape and center of mass at 1034 cm^{-1} (peak maximum of the *Q* branch near 1033 cm^{-1}).

The subset selection procedure of Carpenter and Small[24] was used to select 8000 of these ethanol-inactive interferograms for use in the training set. The remaining 160108 interferograms were placed in prediction set **I**. In an attempt to account for changes in the IR background radiance from day to day and over the intervening approximately four months between the open-air experiments, the selection of these 8000 training interferograms was partitioned into six groups. For the first open-air experiment, the data were subdivided according to the day of collection. For days one to four, 800, 1700, 1700, and 800 interferograms were selected, respectively, for inclusion in the training set. For the second open-air experiment, the ethanol-inactive data consisted only of ammonia releases and various backgrounds acquired when no sample vapors were being released. In this case, the data were subdivided according to these two groups, with 1000 background and 2000 ammonia interferograms being selected for the training set.

Selection of the data in the ethanol-active category was complicated by the nature of data collected in an open-air experiment. In this environment, there was no guarantee that the vapor analyte was within the FOV of the spectrometer, even if it was known that a analyte vapor release was being made. For this reason, the ethanol-active data were visually inspected for the presence of the ethanol signature. This was accomplished in four steps. First, a single-beam spectrum was computed from each interferogram collected during the ethanol releases. Second, this computed spectrum was normalized to unit area. Third, a similarly processed background spectrum collected before the start of the release was subtracted from the ethanol containing spectrum. Fourth, the resulting difference spectrum was inspected for the presence of the ethanol signature. The Fourier processing step included triangular apodization and Mertz phase correction. This inspection procedure yielded a pool of ethanol-active interferograms for inclusion in the training set and prediction set **I**. The subset selection procedure of Carpenter and Small[24] was again used to select 8000 of these ethanol-active interferograms for use in the training set. The remaining 49902 interferograms were placed in prediction set **I**. The subset selection was performed in two groups. For the first and second open-air experiments, respectively, 5000 and 3000 interferograms were selected for inclusion in the training set. A summary of the number of interferograms is furnished in Table 5 for the training set and prediction set **I** corresponding to the various data subsets. In the rightmost columns of Tables 2 and 3 are listed the number of interferograms that were assigned to the data subsets for each of the 38 experimental runs.

The nine digital filtering/interferogram segment optimized combinations from data set **A** and listed in Table 6 were applied to data set **B**. Filters were recomputed with interferogram data from the Brunswick instrument to match the parameters in Table 4. Piecewise linear discriminants were computed with the training set of data set **B**, and the resulting discriminants were applied to prediction set **I**. The corresponding training and prediction results are listed in Table 8 in a manner analogous to those presented previously in Table 6.

Inspection of Table 8 reveals excellent results with each of the three data analysis approaches in terms of training results and overall classification results with prediction set **I**. The two-filter strategy yields the greatest number of correct predictions, although the results are only slightly better than those obtained with the single ethanol filter on a 120-point interferogram segment. The results obtained with the single filter on a 60-point interferogram segment are slightly worse overall, particularly in the area of false detections.

Table 8. Pattern Recognition Results for Open-Air Data Set B

Filter(s) used[a]	Segment[b]	Correct ethanol detections (training)	Correct ethanol detections (Pred. **I**)	False ethanol detections (Pred. **I**)	Total correct classifications (Pred. **I**)
Ethanol filter and 60-point segment					
1[c]	51-110	7978 (99.7%)	49434 (99.1%)	4177 (2.6%)	205365 (97.9%)
2	51-110	7963 (99.5%)	49213 (98.6%)	1088 (0.7%)	208233 (99.2%)
3	51-110	7967 (99.6%)	49372 (98.9%)	2744 (1.7%)	206736 (98.5%)
Ethanol filter and 120-point segment					
1	26-145	8000 (100%)	49736 (99.7%)	1180 (0.7%)	208664 (99.4%)
2	51-170	7997 (99.96%)	49667 (99.5%)	879 (0.5%)	208896 (99.5%)
3[c]	26-145	8000 (100%)	49784 (99.8%)	919 (0.6%)	208973 (99.5%)
Ethanol and ammonia filters with total segment of 120 points					
2 10	51-110 26-85	7987 (99.8%)	49591 (99.4%)	679 (0.4%)	209020 (99.5%)
3[c] 12	51-110 26-85	8000 (100%)	49851 (99.9%)	599 (0.4%)	209360 (99.7%)
1 8	51-110 51-110	7967 (99.6%)	49313 (98.8%)	417 (0.3%)	209004 (99.5%)

[a]Refers to specifications of corresponding filter numbers in Table III.

[b]Starting and ending interferogram points where point of ZPD = 1.

[c]Discriminant applied to Prediction Set **II**.

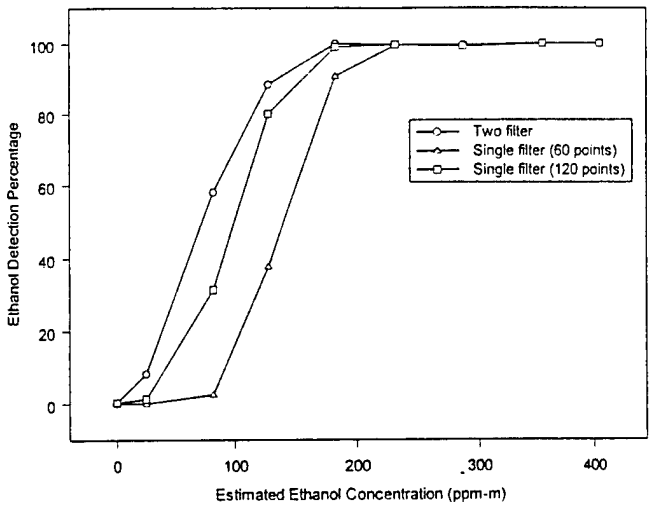

Figure 4. Ethanol Detection Percentage for Three Discriminants as a Function of Estimated Path-Averaged Ethanol Concentration for Prediction Set II

Statistical comparisons of the classification results for prediction set **I** were performed as described previously with data set **A**. The ethanol detection percentage for the two-filter analysis was not significantly greater than that achieved by the other two methods. However, the false detection rates were significantly lower at probabilities of 0.07 and 0.02 when compared to the results obtained with the 60-point and 120-point single-filter methods, respectively.

The discriminant that produced the best training results with each filtering method was next applied to prediction set **II**. These discriminants are indicated by a footnote in Table 8. For the single filter and 120-point segment, two discriminants tied for the best training result. In this case, the discriminant that produced the best total classification result with prediction set **I** was selected for application to prediction set **II**.

For each of the three selected discriminants, Figure 4 plots the ethanol detection percentage as a function of estimated path-averaged concentration. The ethanol/ammonia filter with 120-point segment detection results are displayed as open circles in Figure 4. The single ethanol filter with 120-point segment detection percentages are shown in Figure 4 as open boxes. The single ethanol filter with 60-point segment is illustrated with open triangles in Figure 4. To generate this plot, the times at which the ethanol flow rate changes are mapped onto the corresponding data acquisition times for the interferograms. For the nine estimated ethanol path-averaged concentration levels of 0, 25, 82, 128, 183, 231, 287, 355, and 405 ppm-m, the corresponding numbers of interferograms are 1499, 690, 601, 687, 442, 576, 607, 847, and 51, respectively. For each of these groups, the number of interferograms producing discriminant scores > 0 (i.e., indicating an ethanol detection) is tabulated and the corresponding detection percentage is computed.

Inspection of Figure 4 reveals that each of the discriminants achieves a detection rate close to 100% at concentrations above 200 ppm-m. However, the results differ at that point. Below 200 ppm-m, the two-filter discriminant produces the greatest detection sensitivity, followed by the single-filter discriminants based on 120 and 60 points, respectively. Improved detection sensitivity is observed in the Figure 4 as a slower decrease in ethanol detection percentage with decreasing concentration. All of the discriminants produce a detection percentage of zero when the ethanol concentration is zero. The time trace of the two-filter discriminant response is illustrated as a solid line in Figure 5 with the ordinate scale on the left of the graph. Figure 5 plots the discriminant scores for prediction set **II** as a function of interferogram sequence number for the course of the experimental run. The two-filter discriminant is also used to produce the results in Figure 4. As noted previously, positive discriminant scores indicate an ethanol detection. Overlaid as dotted lines on the Figure 5 plot are the estimated ethanol and ammonia path-averaged concentration levels with the assoicated ordinate scale on the right side of the graph. It is clear from an inspection of this plot that the ethanol detection becomes more challenging as the ethanol concentration drops below that of ammonia.

4. CONCLUSIONS

The results presented in this study clearly show the benefits of employing multiple digital filters in interferogram analysis. The benefits occur in situations for which a vapor analyte signature becomes increasingly overwhelmed by the overlapping signals arising from spectral interferences. In examination of laboratory and open-air data, the combined ethanol and ammonia filter exhibits an improvement in detection sensitivity relative to either of the approaches based on a single filter. This investigation also illustrates that optimization of digital filtering and interferogram segment parameters with laboratory data can successfully be applied to data collected in the open-air scenarios.

The strategy used in this study to evaluate the three filtering approaches was limited, because a full-scale optimization was not performed on the segment lengths used with each filter. Therefore, to equalize the impact of dimensionality on the pattern recognition results, a fixed segment length of 120 points was used as based on the results of a previous study. This dictated that the individual segments in the two-filter approach had to be less than 120 points. In this case, equal segments of 60 points were used. A parallel set of pattern recognition results based on a single filter and a 60-point segment were compiled for a direct comparison with the two-filter approach. Classification results obtained with both laboratory and open-air data indicated that with a single ethanol filter, the 120-point segment offered greater detection sensitivity than the 60-point segment. This was rationalized simply due to a longer integration of the ethanol signal. However, this also suggested that the optimal implementation of the two-filter approach could require a total segment longer than 120 points. Such an implementation would demand a more elaborate optimization strategy than the one currently employed. A formal numerical optimization strategy to address this issue will be the focus of future research efforts.

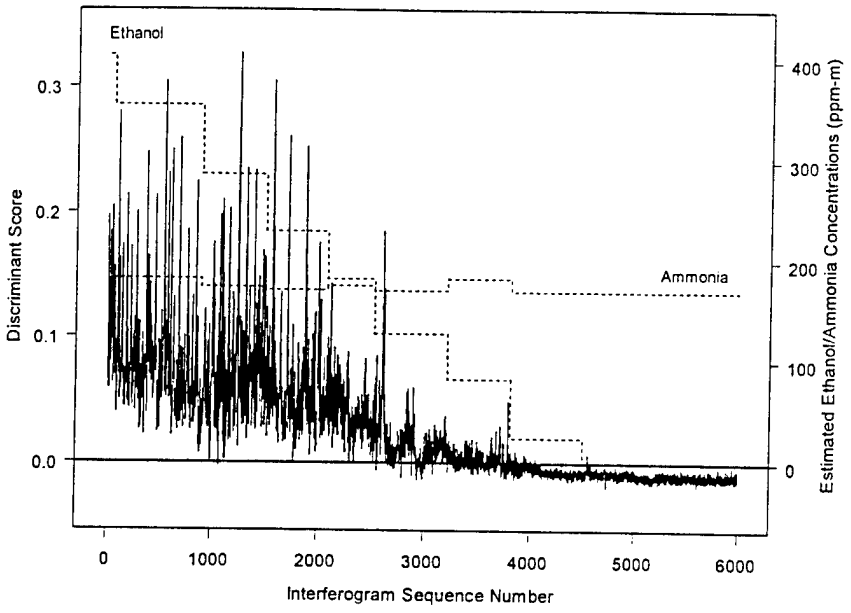

Figure 5. **Discriminant Scores for Prediction Set II for Ethanol/Ammonia Filters with a Total Segment Length of 120 Points**

LITERATURE CITED

1. R.M. Hammaker, W.G. Fateley, C.T. Chaffin, T.L. Marshall, M.D. Tucker, V.D. Makepeace, and J.M. Poholarz, "FT-IR Remote Sensing of Industrial Atmospheres for Spatial Characterization," Applied Spectroscopy Vol. 47, No. 9, pp 1471-1475 (1993).

2. Timothy L. Marshall, Charles T. Chaffin, Robert M. Hammaker, and William G. Fateley, "An Introduction to Open-Path FT-IR Atmospheric Monitoring," Environmental Science and Technology Vol. 28, No. 5, pp 224A-232A (1994).

3. Linda Ingling and Thomas L. Isenhour, "Spectral Matching Quantitative Open-Path Fourier-transform Infrared Spectroscopy," Field Analytical Chemistry and Technology Vol. 3, No. 1, pp 37-43 (1999).

4. Roger J. Combs, "Thermal Stability Evaluation for Passive FTIR Spectrometry," Field Analytical Chemistry and Technology Vol. 3, No. 2, pp 81-94 (1999).

5. C.T. Chaffin, Jr., T.L. Marshall, and N.C. Chaffin, "Passive FTIR Remote Sensing of Smokestack Emissions," Field Analytical Chemistry and Technology Vol. 3, No. 2, pp 111-115 (1999).

6. Arjun S. Bangalore, Gary W. Small, Roger J. Combs, Robert B. Knapp, and Robert T. Kroutil, "Automated Detection of Methanol Vapor by Open Path Fourier Transform Infrared Spectrometry," Analytica Chimica Acta Vol. 297, No. 3, pp 387-403 (1994).

7. Arjun S. Bangalore, Gary W. Small, Roger J. Combs, Robert B. Knapp, Robert T. Kroutil, Carol A. Traynor, and John D. Ko, "Automated Detection of Trichloroethylene by Fourier Transform Infrared Remote Sensing Measurements," Analytical Chemistry Vol. 69, No. 2, pp 118-129 (1997).

8. Cheryl L. Hammer, Gary W. Small, Roger J. Combs, Robert B. Knapp, and Robert T. Kroutil, "Artificial Neural Networks for the Automated Detection of Trichloroethylene by Passive Fourier Transform Infrared Spectrometry," Analytical Chemistry Vol. 72, No. 7, pp 1680-1689 (2000).

9. Frederick W. Koehler, IV, Gary W. Small, Roger J. Combs, Robert B. Knapp, and Robert T. Kroutil, "Calibration Transfer in the Automated Detection of Acetone by Passive Fourier Transform Infrared Spectrometry," Applied Spectroscopy Vol. 54, No. 5, pp 706-714 (2000).

10. Ronald E. Shaffer, Gary W. Small, Roger J. Combs, Robert B. Knapp, and Robert T. Kroutil, "Experimental Design Protocol for the Pattern Recognition Analysis of Bandpass Filtered Fourier Transform Infrared Interferograms," Chemometrics and Intelligent Laboratory Systems Vol. 29, No. 1, pp 89-108 (1995).

11. P. Hariharan, Basics of Interferometry, Chapter 3, Academic Press, Boston, MA, 1992.

12. R.T. Kroutil, M. Housky, and G.W. Small, "Real-Time Data-Collection Programs for a Commercial Passive FT-IR Remote Sensor," Spectroscopy Vol. 9, No. 2, pp 41-47 (1994).

13. CRC Handbook of Chemistry and Physics, 53rd Edition, Chemical Rubber Company, Cleveland, OH, 1972.

14. O. Sohnel and P. Novotny, Densities of Aqueous Solutions of Inorganic Substances, p 32, Elsevier, New York, NY, 1985.

15. Paul E. Field, Roger J. Combs, and Robert B. Knapp, "Equilibrium Vapor Cell for Quantitative IR Absorbance Measurements," Applied Spectroscopy Vol. 50, No. 10, pp 1307-1313 (1996).

16. M. Hirata, S. Ohe, and K. Nagahama, Computer Aided Data Book Vapor-Liquid Equilibria, p 799, Elsevier, New York, NY, 1975.

17. Roger J. Combs, Robert T. Kroutil, and Robert B. Knapp, M21 Interface and Data Acquisition Software (MIDAS), ERDEC-TR-298, U.S. Army Edgewood Research, Development and Engineering Center, Aberdeen Proving Ground, MD, April 1996, UNCLASSIFIED Report (AD-B211 591).

18. Charles T. Chaffin, Jr., and Timothy L. Marshall, "Generating Well-characterized Chemical Plumes for Remote Sensing Research," in Proceedings of SPIE Conference on Electro-Optical Technology for Remote Chemical Detection and Identification III, Eds. M. Fallahi and E. Howden, Vol. 3383, pp 113-123, SPIE, Orlando, FL, April 1998.

19. J. Ballard, J.J. Remedios, and H.K. Roscoe, "The Effect of Sample Emission on Measurements of Spectral Parameters Using a Fourier Transform Absorption Spectrometer," Journal of Quantitative Spectroscopy and Radiative Transfer Vol.48, Nos. 5-6, pp 733-741 (1992).

20. Gary W. Small, Amy C. Harms, Robert T. Kroutil, John T. Ditillo, and William R. Loerop, "Design of Optimized Finite Impulse Response Digital Filters for Use with Passive Fourier Transform Infrared Interferograms," Analytical Chemistry Vol. 62, No. 17, pp 1768-1777 (1990).

21. Thomas F. Kaltenbach and Gary W. Small, "Development and Optimization of Piecewise Linear Discriminants for the Automated Detection of Chemical Species," Analytical Chemistry Vol. 63, No. 9, pp 936-944 (1991).

22. Ronald E. Shaffer and Gary W. Small, "Improved Response Function for the Simplex Optimization of Piecewise Linear Discriminants," Chemometrics and Intelligent Laboratory Systems Vol. 32, No. 1, pp 95-109 (1996).

23. Ronald E. Shaffer and Gary W. Small, "Comparison of Optimization Algorithms for Piecewise Linear Discriminant Analysis: Application to Fourier Transform Infrared Remote Sensing Measurements," Analytica Chimica Acta Vol. 331, No. 3, pp 157-175 (1996).

24. Scott E. Carpenter and Gary W. Small, "Selection of Optimum Training Sets for Use in Pattern Recognition Analysis of Chemical Data," Analytica Chimica Acta Vol. 249, No. 2, pp 305-321 (1991).

25. Robert T. Kroutil, John T. Ditillo, and Gary W. Small, "Signal Processing Techniques for Remote Infrared Chemical Sensing," in Computer-Enhanced Analytical Spectroscopy, Ed. H.L.C. Meuzelaar, Vol. 2, Plenum Publishing, New York, NY, pp 71-11, 1990.

26. Daniel MacDougall, Francis J. Amore, Geraldine V. Cox, Donald G. Crosby, Francis L. Estes, David H. Freeman, William E. Gibbs, Glen E. Gordon, Lawrence H. Keith, Joginder Lal, Ralph R. Langner, Nina I. McClelland, Wendell F. Phillips, Robert B. Pojasek, Robert E. Sievers, Robert G. Smerko, David C. Wimert, Warren B. Crummett, Robert Libby, Herbert A. Laitinen, Michael M. Reddy, and John K. Taylor, "Guidelines for Data Acquisition and Data Quality Evalution in Environmental Chemistry," Analytical Chemistry Vol. 52, No. 14, pp 2242-2249 (1980).